Choroid plexus enlargement in inflammatory multiple sclerosis: 3T MRI and translocator protein PET evaluation

Vito Ag Ricigliano, Emanuele Morena, Annalisa Colombi, Matteo Tonietto, Mariem Hamzaoui, Emilie Poirion, Michel Bottlaender, Philippe Gervais, Celine Louapre, Benedetta Bodini, et al.

Choroid plexus enlargement in inflammatory multiple sclerosis: 3T MRI and translocator protein PET evaluation

Vito AG RICIGLIANO, MD[1], Emanuele MORENA, MD[1], Annalisa COLOMBI, MD[1], Matteo TONIETTO, PhD[1,2], Mariem HAMZAOUI, MSc[1], Emilie POIRION, PhD[1,3], Michel BOTTLAENDER, MD, PhD[2], Philippe GERVAIS, PhD[2], Celine LOUAPRE, MD, PhD[1,4], Benedetta BODINI, MD, PhD[1,5], Bruno STANKOFF, MD, PhD[1,5]

[1]Sorbonne Université, Paris Brain Institute, ICM, CNRS, Inserm, 75013 Paris, France

[2]Université Paris-Saclay, CEA, CNRS, Inserm, BioMaps, Service Hospitalier Frédéric Joliot, 91400 Orsay, France

[3]Service d'Imagerie Médicale, Hôpital Fondation Adolphe de Rothschild, 75019 Paris, France

[4]Neurology Department, Pitié-Salpêtrière Hospital, APHP, 75013 Paris, France

[5]Neurology Department, St Antoine Hospital, APHP, 75012 Paris, France

Corresponding author*:*

Bruno Stankoff, MD, PhD

ICM, Hôpital Pitié-Salpêtrière,

47, Boulevard de l'Hôpital,

75013 Paris, France

Phone: +33157274463

E-mail: bruno.stankoff@aphp.fr

Article type: Original Research

Summary statement: A combination of 3D MRI and translocator protein PET demonstrated enlarged and inflamed choroid plexuses in patients with multiple sclerosis (MS), representing a potential imaging marker for active MS.

Key results:

Among 97 patients with multiple sclerosis (MS) and 44 controls who underwent a 3T brain MRI and translocator protein PET study, patients had 35% larger choroid plexuses than controls (*P*=.004).

Choroid plexus enlargement was higher in patients with gadolinium-enhancing lesions (*P*<.001) and correlated with higher white matter lesion load (r:0.39;*P*<.001). Choroid plexus size correlated also with neuroinflammation measured by ^{18}F-DPA-714 PET in white matter (r:0.5;*P*=.005) and thalami (r:0.44;*P*=.04), and with 4-year annualized relapse rate (r:0.37;*P*=.005).

List of all abbreviations: MS = multiple sclerosis; RRMS = relapsing-remitting multiple sclerosis; PMS = progressive multiple sclerosis; CP = choroid plexus; TSPO = translocator protein; FDG = fluorodeoxyglucose; ARR = annualized relapse rate; NAWM = normal-appearing white matter; ROI: region of interest.

Abstract

Background: Choroid plexuses (CPs) have been suggested as a key gateway for inflammation in experimental autoimmune encephalitis, but we lack *in vivo* evidence of their involvement in multiple sclerosis (MS).

Purpose: To assess CP volumetric and inflammatory changes in patients with MS *versus* healthy controls (HCs).

Materials and Methods: Secondary analysis of 97 patients (61 relapsing-remitting, RRMS, 36 progressive) and 44 HCs undergoing a prospective 3T brain MRI study (May 2009-September 2017, EudraCTNumber:2008-004174-40;ClinicalTrials.gov:NCT02305264, NCT01651520); a subgroup of 37 patients and 19 HCs also underwent translocator protein ^{18}F-DPA-714 PET for neuroinflammation. Relapses and disability scores were collected at baseline and over 2 years. CPs were manually segmented on 3DT1-weighted images; other brain volumes were additionally segmented. Volumes were expressed as ratio of intracranial volume. ^{18}F-DPA-714 distribution volume ratio was quantified in parenchymal regions, whereas standardized uptake value was used for CP inflammation. Multivariable linear regressions were fitted to assess: i) CP volumetric and inflammatory differences between MS and HCs; ii) correlations between CP volume and lesion load, brain volumes, ^{18}F-DPA-714 uptake and annualized relapse rate (ARR).

Results: 97 patients (mean age:42±12 years, 49 women) and 44 HCs (mean age:39±14 years, 23 women) underwent MRI; 37 patients and 19 HCs underwent PET. CPs were 35% larger in MS (mean value:15.9±4.5x10^{-4}) *versus* HCs (mean value:11.8±3.8x10^{-4};*P*=.004). Subgroup analysis confirmed greater volume in RRMS (mean value:15.5±4.6x10^{-4};*P*=.008). CP enlargement was higher in MRI-active patients (mean value in gadolinium-positive patients:18.2±4.9x10^{-4}, mean value in gadolinium-negative patients:14.9±4x10^{-4};*P*<.001) and correlated with white matter lesion load (r:0.39;95%CI=0.20:0.55;*P*<.001), thalamic and NAWM ^{18}F-DPA-714 binding (r:0.44;95%CI=0.22:0.72;*P*=.04, and r:0.5;95%CI=0.20:0.71;*P*=.005). Moreover, it correlated with ARR in RRMS (r:0.37;95%CI=0.1:0.55;*P*=.005). Finally, patients showed 18.5% higher CP ^{18}F-DPA-714 uptake (mean

value in MS:0.778±0.23, mean value in HC:0.635±0.15;*P*=.01), correlating with CP volume in RRMS (r:0.57;95%CI=0.37:0.73;*P*=.009).

Conclusion: CPs are enlarged and inflamed in MS, particularly RRMS with inflammatory profiles; CP volumetric analysis could represent an MS imaging marker.

Introduction

In multiple sclerosis (MS), the biological mechanisms underlying central nervous system (CNS) attack are not yet fully understood.[1] A predominant hypothesis is that an antigen-specific immune activation occurs at first in the periphery and is then transferred into the CNS, mainly through lymphocyte migration across the blood brain barrier.[2,3] The contribution of an altered blood to cerebrospinal fluid (CSF) barrier and of a CSF clearance deficit remains debated.[4,5]

The choroid plexuses (CPs) are primarily responsible for the production of the CSF but are also part of the blood-CSF barrier[6] and contribute to the regulation of CNS immunosurveillance.[7,8] In the murine model of experimental autoimmune encephalomyelitis (EAE), inflammation in the CPs and CSF precedes the formation of parenchymal inflammatory infiltrates and the development of demyelinating white matter (WM) lesions,[9,10] leading to the hypothesis that CP involvement might be an early phenomenon in human demyelinating diseases.

In post-mortem studies, patients with MS show more antigen-presenting cells in CP stroma, an infiltration of peripheral leukocytes,[11,12] a disruption of tight junctions in the CP epithelium,[13] and an endothelial overexpression of adhesion molecules involved in lymphocyte migration.[12] Despite the body of evidence available from translational and neuropathologic studies, we still lack an *in vivo* demonstration that CPs could be involved in the inflammatory process characterizing MS.

Non-invasive evaluation of CP morphology with 3D high-field MRI has been recently performed for non-inflammatory neurological diseases.[14,15] In MS, a higher brightness of CP on T1 post-gadolinium sequences and concurrent MS and CP papilloma have been described.[16,17] However, to our knowledge, the relationship between inflammation and CP morphology has never been assessed. In the present study, we combined 3D MRI techniques with translocator protein (TSPO) and fluorodeoxyglucose (FDG) PET,[18,19] to explore the alterations of the CPs and their relationship with inflammation on a large sample of patients with MS and age- and sex-matched healthy controls (HC).

Materials and Methods

Study design

For the three prospective studies (EudraCT Number:2008-004174-40;ClinicalTrials.gov:NCT02305264, NCT01651520) on which this secondary analysis was performed, written informed consent was obtained from all participants and the studies were approved by the local ethic committees. The full study protocols can be accessed via https://www.clinicaltrialsregister.eu and https://clinicaltrials.gov. Data generated or analyzed during the study are available from the corresponding author by request.

The study included a convenience series of patients with relapsing-remitting (RRMS) or progressive MS (PMS) (age≥18 years, 1 month after corticosteroid/immunosuppressive therapy), and age- and sex-matched HCs. These were included from three neuroimaging protocols between May 2009 and September 2017 at the Paris Brain Institute, France. Exclusion criteria were: i) impossibility to perform a PET and MRI exam for any reason (e.g. claustrophobia, pace-maker or intra-ocular foreign body); ii) severe or uncontrolled renal, hepatic, hematological, gastrointestinal pulmonary or cardiac disease; iii) other chronic neurological disease; iii) prior participation in other research protocols or clinical care in the last year such that radiation exposure would exceed the annual guidelines; for women: pregnancy, lactation, lack of efficient contraception.
At study entry, patients with MS were scored on the Expanded Disability Status Scale (EDSS) and divided into three groups: no treatment, on first-line, or second-line treatment. Moreover, the number of relapses and EDSS in the 2 years preceding and following inclusion were collected.

A subgroup underwent a ^{18}F-DPA-714 PET scan at study entry. After genotyping of the rs6971 polymorphism of the TSPO gene,[20] low-affinity binders were excluded from further analysis, that being an additional exclusion criterion in this neuroimaging protocol. The remaining 37 patients with MS and 19 HCs have been reported in a prior article that dealt with the generation of PET-derived individual maps of innate immune cell activation,[18] whereas the present article focuses on the analysis of the choroid plexuses. From this group, all patients and half of the HC (n=9) were planned to undergo a ^{18}F-FDG PET scan within the 2 weeks preceding or following the ^{18}F-DPA-714 exam (ClinicalTrials.gov:NCT02305264). 3 subjects (1 MS,

2 HC) withdrew after the ^{18}F-DPA-714 PET scan for personal reasons, leaving a total of 36 patients with MS and 7 HCs for the ^{18}F-FDG PET part (**Fig 1**).

Image acquisition

Patients were scanned on a 3T MRI system with a 32-channel head coil (60 patients with MS/32 HCs on a Siemens TRIO, while 37 patients with MS/12 HCs on a Siemens PRISMA). Acquired sequences included 3D T1-weighted magnetization-prepared rapid gradient echo (MPRAGE, repetition time (TR)/echo time (TE):2300/2.98 ms), T2-weighted (TR/TE:4100/83 ms), and pre- and post-gadolinium (Dotarem, Guerbet Diagnostic Imaging) T1 spin-echo (TR/TE:700/14 ms). ^{18}F-DPA-714 and ^{18}F-FDG PET images were acquired on a Siemens ECAT high-spatial-resolution research tomograph (HRRT; CPS Innovations) with a 90-min or 60-min dynamic acquisition, respectively (**Supplemental 1**).

Post-processing

In patients with MS, WM lesions were contoured on T2-w scans, and gadolinium-enhancing lesions on post-gadolinium T1-SE scans using Jim (v6.0,http://www.xinapse.com/). Binary lesion masks were aligned to 3D-T1 MPRAGE scans with FLIRT (v5.0.9,http://fsl.fmrib.ox.ac.uk/).[21] After lesion-filling, Freesurfer (v6.0,http://surfer.nmr.mgh.harvard.edu/) was used on 3D-T1 MPRAGE scans to estimate total intracranial volume (TIV) and to segment gray matter, WM and CSF, with manual correction when necessary.

The CPs of the lateral ventricles were manually segmented by three trained neurologists independently (VAGR, EM, AC) (3 year expertise in MRI processing) and systematically corrected by a fourth neurologist (BB, 12 year expertise in MRI processing) on the sagittal, axial and coronal plans of the 3D-T1 MPRAGE scans using ITK-SNAP (v3.8.0,http://www.itksnap.org/), and their volume was calculated (**Fig 2a-b**). Readout sessions were performed by each of the three segmenting neurologists with an interval of one week. The status of the subject (HC or MS) was blinded to the fourth neurologist who corrected the segmentations. In case of disagreement, images were reviewed by all neurologists at once in a common session, and a final decision on the segmentation was taken by majority. Freesurfer CP segmentation was also performed as a

crosscheck. The CPs of the third and fourth ventricles were not included in the analysis, given their inconstant visualization.[22]

The following regions of interest (ROIs) were defined on T1-w scans using Freesurfer: (i) whole brain without ventricles; (ii) cortex; (iii) WM; (iv) thalami, given their role as a crucial barometer of diffuse parenchymal damage in MS; and (v) ventricles. In patients with MS, three additional ROIs were selected: (i) T2-w lesions; (ii) perilesions, corresponding to the 2mm rim surrounding each lesion; (iii) normal-appearing WM (NAWM), defined as the WM without lesions and perilesions on T2-w scans. The volume of CPs and other ROIs was divided by the TIV to obtain the corresponding normalized value.

Voxel-wise ^{18}F-DPA-714 distribution volume ratio (DVR) parametric maps were obtained using the Logan graphical analysis based on reference region.[23] All ROIs were aligned to the corresponding PET images using FLIRT[22] to extract the mean DVR values. Mean ^{18}F-DPA-714 and ^{18}F-FDG uptake inside the CPs were calculated as the average standardized uptake value (SUV),[24,25] after performing partial volume correction of the CPs with the single target correction method in PETPVC (v1.2.0-b,https://github.com/UCL/PETPVC; **Supplemental 1**).[26]

Statistical Analysis

Statistical analyses were performed with STATA (v14.0,https://www.stata.com/), considering two-sided $P<.05$ as significant. Sample size was calculated to detect a large effect (Cohen's $d\geq 0.8$) for the difference in mean CP volume between groups, with power=80%, alpha=0.05.

Wilcoxon-Mann-Whitney and Fisher's exact tests were used as appropriate to assess differences in age, sex, TSPO affinity and MRI scanner between patients with MS and HCs, and in disease duration and treatment between RRMS and PMS. Ordered logistic regressions were used for differences in EDSS between MS subgroups, and for the association of CP volume with 4-year annualized relapse rate (ARR, from 2 years before to 2 years after inclusion), baseline EDSS and 2-year EDSS change.

Multivariable linear regressions were fitted to test:

1) differences between the whole MS group or subgroups and HC, and between MS subgroups, regarding: i) CP volume, adjusting for ventricular and brain volume; ii) CP ^{18}F-DPA-714 SUV_{60-90} and ^{18}F-FDG SUV_{45-60}, adjusting for CP volume; iii) CP volume between gadolinium-positive and gadolinium-negative patients with MS;
2) correlations between CP volume and: i) age, sex, disease duration, ROI volumes (adjusting for brain volume in the last case); ii) ^{18}F-DPA-714 DVR of parenchymal brain ROIs; ii) CP ^{18}F-DPA-714 SUV_{60-90} and ^{18}F-FDG SUV_{45-60}.

Pearson's r was used to assess the strength of correlations, the inter-rater reliability and the manual-Freesurfer correlation of CP segmentation. Regressions were adjusted for: i) age and sex; ii) MRI scanner when MRI variables were tested; iii) brain volume and TSPO affinity in the subgroup receiving DPA; iv) treatment in patients with MS. Results were Bonferroni corrected for multiple comparisons and post-hoc analyses were repeated on RRMS and PMS subgroups.

Results

Patient Characteristics

We evaluated 97 patients with MS (61 with relapsing-remitting RRMS and 36 with progressive PMS) and 44 age- and sex-matched HC. Patients with MS and HC (**Table 1**) were not different in terms of age (MS: mean age:42±12 years, HC: mean age:39±14 years, *P*=.18), sex (MS: 49 women, HC: 23 women, *P*=.47) and 3T MRI scanner used (MS: TRIO/PRISMA 60/37, HC: TRIO/PRISMA 32/12, *P*=.14). Median disease duration was 4.8 years and was higher in PMS compared with RRMS (*P*=.04). Median EDSS was 3, with higher scores in PMS (*P*<.001). Clinically active disease, defined as 2-year retrospective ARR≠0, was present in 55 out of 97 patients with MS (57%). Treatment type differed between MS types (*P*<.001), with a greater number of untreated patients with PMS compared with RRMS.

The subgroup receiving DPA was composed of 41 patients (13 RRMS and 28 PMS) and 20 HC. After genotyping of the rs6971 polymorphism of the TSPO gene, 5 low-affinity binders (4 MS, 1 HC) were excluded from further analysis, which left 37 patients with MS and 19 HCs. In this subgroup, no difference was present between MS and HC in age (47±14 for MS; 48±11 for HC; *P*=.92), sex (21 women among patients with MS; 13 women among HC; *P*=.56), TSPO affinity (proportion high/mixed-affinity binders [HAB/MAB]: 22/15 for MS, 10/9 for HC; *P*=.42) and scanner (*P*=.41). Disease duration, EDSS and treatment were different between RRMS and PMS (*P*=.03, *P*<.001, and *P*<.001, respectively). Clinically active disease was present in 16 out of 37 patients with MS (43%).

Patients with MS have larger choroid plexuses compared with HC

Manually-segmented CP volumes were highly consistent across different operators and correlated with Freesurfer segmentation (r=0.89; 95% CI=0.86:0.92; *P*<.001; r=0.55; 95% CI=0.42:0.65; *P*<.001, respectively). Choroid plexus volume, expressed as ratio of TIV, was 35% greater in patients with MS compared with HC (mean value in MS:15.9±4.5x10^{-4}; mean value in HC:11.8±3.8x10^{-4}; coeff:4x10^{-4}; *P*<.001). In both patients with MS and HC, CP volume was strongly correlated with ventricular volume (MS:

r:0.55; 95% CI=0.40:0.68; coeff:0.03; *P*<.001; HC: r:0.50; 95% CI=0.24:0.70; coeff:-0.04; *P*=.001), but not with age (MS: *P*=.49; HC: *P*=.49) or sex (MS: *P*=.58; HC: *P*=.29).

After adjusting for ventricular and brain volume, CP volume remained higher in patients with MS compared with HC (coeff:22.5x10^{-5}; *P*=.004)(**Fig 2c**). In the analysis of MS subgroups, only patients with RRMS showed greater CP volume compared with HC (mean value in RRMS:15.5±4.6x10^{-4}; coeff:21.6x10^{-5}; *P*=.008; mean value in PMS:16.5±4.3x10^{-4}; coeff:7x10^{-5}; *P*=.24), but no difference in CP volume was found when testing MS subgroups against each other (*P*=.47)(**Fig 2d**).

Enlarged choroid plexuses are associated with lower brain volume

In patients with MS, larger CPs were associated with lower volume in the whole brain (r:-0.33; 95% CI=-0.49:-0.14; *P*=.004)(**Fig 3a**), the thalami (r:-0.37; 95% CI=-0.53:-0.19; *P*<.001) and the NAWM (r:-0.46; 95% CI=-0.61:-0.29; *P*=.004) but not in the cortex (r:-0.26; 95% CI=-0.38:0.01; *P*>.99)(**Fig 3b-d**). Post-hoc subgroup analysis of RRMS and PMS showed similar results (RRMS: whole brain: r:-0.29; 95% CI=-0.50:-0.03; *P*=.02; thalami: r:-0.45; 95% CI=-0.63:-0.23; *P*=.002; NAWM: r:-0.52; 95% CI=-0.68:-0.30; *P*=.005; PMS: whole brain: r:-0.38; 95% CI=-0.63:-0.06; *P*=.02; NAWM: r:-0.51; 95% CI=-0.72:-0.22; *P*=.004).

In HC, CP volume was not associated with any ROI volumes (whole brain: *P*=.18; thalami: *P*>.99; WM: *P*>.99; cortex: *P*>.99)(**Table 2**).

Choroid plexus enlargement is associated with brain inflammation and relapses in MS

Choroid plexus volume correlates with T2 lesion load and is higher in patients with active MS.

Enlarged CPs were associated with greater T2-w WM lesion volume in the whole MS group (r:0.39; 95% CI=0.20:0.55; coeff:8.35; *P*<.001)(**Fig 4a**) and in RRMS (r:0.48; 95% CI=0.26:0.65; coeff:11.1; *P*=.001), but not in PMS (*P*=.27). Gadolinium-enhancing lesions were present in 26 RRMS and 5 patients with PMS. In the whole MS group, patients with at least one gadolinium-enhancing lesion had 22% larger CPs (mean volume:18.2±4.9x10^{-4}) compared with those without active lesions (mean volume:14.9±4x10^{-4}; coeff:3.7x10^{-4}; *P*<.001)(**Fig 4b).** This result was confirmed on both RRMS (coeff:3.9x10^{-4}; *P*=.002) and PMS (coeff:4.98x10^{-4}; *P*=.04).

In the whole MS group, CP volume did not correlate with EDSS, 2-year EDSS change, disease duration or 4-year ARR (*P*=.58, *P*>.99, *P*=.20 and *P*=.19, respectively). In subgroup analysis, a higher 4-year ARR, reflecting a more active disease, was associated with larger CPs in RRMS (r:0.37; 95% CI=0.10:0.55; coeff:$1.36x10^{3}$; *P*=.005)(**Fig 4c**) but not in PMS (*P*=.66). More in detail, in the RRMS subgroup, patients who experienced ≥1 relapse during the 2-year follow-up (n=18) had larger CPs at baseline (mean volume: $17.5\pm4.9x10^{-4}$) compared to patients who remained stable over time (n=43, mean volume: $14.7\pm4.3x10^{-4}$, *P*=.03).

Enlarged choroid plexuses are associated with greater parenchymal neuroinflammation

In the group receiving DPA, we confirmed that patients with MS had larger CPs compared with HC (29% higher; coeff:$2.42x10^{-4}$; *P*=.03). After adjusting for brain volume, in the group of patients with MS, CP enlargement was associated with higher ^{18}F-DPA-714 binding in the thalami (r:0.44; 95% CI=0.22:0.72; *P*=.04) and the NAWM (r:0.5; 95% CI=0.20:0.71; *P*=.005) but not in the cortex (*P*>.99), in T2-w lesions (*P*>.99)(**Fig 5a)** or perilesions (*P*>.99)(**Fig 5b**).

Results of the post-hoc analysis on MS subgroups showed that in RRMS, larger choroid plexuses correlated with higher ^{18}F-DPA-714 binding in T2-w lesions (r:0.56; 95% CI=0.08:0.86; *P*=.04) and the NAWM (r:0.62; 95% CI=0.07:0.88; *P*=.007). Among patients with PMS, CP enlargement was associated with ^{18}F-DPA-714 binding in the thalami (r:0.67; 95% CI=0.37:0.84; *P*=.001) and the NAWM (r:0.4; 95% CI=0.01:0.69; *P*=.004)(**Table 3**). In HC, CP volume was not associated with ^{18}F-DPA-714 binding in any ROIs (thalami: *P*=.10; WM: *P*=.07; cortex: *P*=.38)(**Table 3**).

Choroid plexuses overexpress TSPO in MS

After controlling for CP volume, the CPs of patients with MS exhibited a 18.5% higher ^{18}F-DPA-714 SUV_{60-90}, compared with HC (mean ^{18}F-DPA-714 SUV_{60-90} in MS:0.778±0.23, mean ^{18}F-DPA-714 SUV_{60-90} in HC:0.635±0.15; coeff:0.14; *P*=.01)(**Fig 5c-d, Fig 6a**). Both high- and mixed-affinity TSPO binder groups had different results (*P*=.004 and *P*=.04, respectively). The results were similar with and without PVC. The analysis of the entire ^{18}F-DPA-714 SUV curves showed that the group differences were observed in the late

frames but not in the initial perfusional frames (P>.99, **Supplemental Fig 1**). In MS subgroup analysis, the ^{18}F-DPA-714 uptake in the CPs differed between MS and HC for RRMS but not for PMS (mean ^{18}F-DPA-714 SUV_{60-90} in RRMS:0.91±0.22; coeff:0.20; *P*=.007; mean ^{18}F-DPA-714 SUV_{60-90} in PMS:0.714±0.21; coeff:0.09; *P*=.12)(**Fig 6b**).

In RRMS, CP size correlated with higher ^{18}F-DPA-714 SUV_{60-90} (r:0.57; 95% CI=0.37:0.73; *P*=.009)(**Fig 6c**), a finding confirmed when removing the two subjects with the lowest and highest value of CP size (*P*=.04), whereas this correlation was not found in PMS (*P*=.39). The interaction between CP volume and RRMS/PMS subgroups confirmed this finding (coeff:-209.70; *P*=.04).

After controlling for CP volume, ^{18}F-FDG SUV_{45-60} in the CPs was not different between patients with MS and HC, neither in the whole MS group (mean ^{18}F-FDG SUV_{45-60} in MS:2.56±0.67, mean ^{18}F- FDG SUV_{45-60} in HC:2.48±0.5; coeff:0.11; *P*=.62)(**Supplemental Fig 1**) nor at the subgroup level (mean ^{18}F- FDG SUV_{45-60} in RRMS:2.58±0.58; coeff:0.14; *P*=.64; mean ^{18}F- FDG SUV_{45-60} in PMS:2.55±0.72; coeff:0.25; *P*=.39). Furthermore, CP size was not correlated with higher ^{18}F-FDG SUV_{45-60} in any MS forms (RRMS: *P*=.99; PMS: *P*=.67).

Discussion

While choroid plexuses (CPs) play an essential role in the homeostasis of the blood-CSF barrier and the recruitment of inflammatory cells into the CNS,[8] few investigations have explored *in vivo* in humans their contribution to MS pathophysiology. In our study of 97 patients with multiple sclerosis (MS) and 44 healthy controls (HCs) who underwent 3T brain MRI and translocator protein PET, patients with MS had 35% larger choroid plexuses than HCs (mean value in MS:15.9±4.5x10^{-4}, mean value in HC:11.8±3.8x10^{-4}, *P*=.004). Moreover, a greater TSPO expression was found in the CPs of patients with MS (mean ^{18}F-DPA-714 SUV_{60-90} in MS: 0.778±0.23, mean ^{18}F-DPA-714 SUV_{60-90} in HC: 0.635±0.15, *P*=.01). Interestingly, CP abnormalities were mainly detected at the relapsing-remitting stage, as attested by a significantly greater CP volume (mean value in RRMS:15.5±4.6x10^{-4}, *P*=.008) and higher CP ^{18}F-DPA-714 uptake compared with HC (mean ^{18}F-DPA-714 SUV_{60-90} in RRMS: 0.91±0.22, *P*=.007), together with a correlation between CP volume and TSPO expression in this subgroup (r:0.57, *P*=.009).

In a recent study, an increased brightness was observed on post-gadolinium T1-weighted sequences in the CPs of patients with MS and neuromyelitis optica spectrum disorder.[17] Importantly, the approach applied by Kim et al[17] was semi-quantitative, as the CPs were enhanced following gadolinium injection in all individuals, with and without disease. In the same study, the CP thickness, evaluated on 2D axial slices, did not significantly differ between patients with MS and controls.[17] This result that seems in contrast with our findings is most likely due to the complex morphology of the CPs, which justifies a rigorous manual segmentation on standardized 3D-MRI acquisitions, as performed here, for accurate volume quantification. In our study, patients with RRMS exhibited enlarged CPs compared with controls, and the difference remained significant when adjusting for ventricular and brain volume. By contrast, in PMS the difference with HC was lost after adjustment, possibly due to a lower statistical power given the smaller sample size, or a more heterogeneous inflammatory component in the CPs.

In post-mortem studies, the CP stroma has shown inflammatory changes, with infiltrating innate cells,[12,27] activated complement deposition and overexpression of adhesion molecules such as VCAM-1.[28] In PMS,

this immune infiltration was moderate and differed with controls only for granulocytes and CD8+ T cells.[11] A deregulation of the HIF-1 pathway, reflecting altered secretory and neuroprotective properties of CPs, has also been described in MS.[29] To what extent inflammatory or secretory changes influence CP volume remains unknown.

Overall, our pathological and imaging findings suggest that the enlarged CP volume in our study may partly be related to an inflammatory component, as reflected by the higher ^{18}F-DPA-714 uptake in CPs. CP inflammatory changes could peak in the relapsing-remitting phase, and subsequently become less pronounced or more heterogeneous at later progressive stages. It is unlikely that increased blood flow in the CPs of patients contribute to the higher CP ^{18}F-DPA-714 uptake measured by PET, as the detailed analysis of SUV curves along all the PET frames did not show a significant group difference in the initial peak, which corresponds to perfusion (Supplemental Fig 1). Few studies have investigated, in mouse and in normal human brain, TSPO expression in the CPs, showing its localization mainly in epithelial cells and macrophages and to a less extent, in vessels.[30,31] Based on these findings, the contribution of vascular binding to the ^{18}F-DPA-714 signal should indeed be minor in this compartment. In addition, post-mortem investigations have shown an ependymal disruption together with scattered microglial infiltration in the CPs of patients with MS,[32] supporting the interpretation that the increase in ^{18}F-DPA-714 uptake is related to inflammatory cells rather than to increased expression by epithelial cells. However, given the lack of imaging/pathology correlative analysis, alternative contributors for the CP ^{18}F-DPA-714 uptake cannot be fully excluded.

Contrasting with ^{18}F-DPA-714 uptake, CP ^{18}F-FDG uptake was not correlated with CP size in RRMS, arguing for a ^{18}F-DPA-714-specific PET signal in the CPs, most likely related to their inflammation. In this scenario, the lack of difference in ^{18}F-FDG uptake between patients and controls may result from the coexistence of a stromal infiltration by macrophages, potentially inducing an increase in FDG uptake, with an epithelial loss in the CPs, that may result in reduced glucose consumption.[32] The presence of innate immune cells with a homeostatic phenotype, characterized by a predominant oxidative metabolism over the glycolytic one,[33] could also explain this result.

Under physiological conditions, CPs act as a unique neuro-immunological interface integrating signals received from the CNS with those coming from circulating immune cells.[8] Following a CNS insult, CPs

allow the trafficking of circulating immune cells towards the CSF, where they can adopt an anti-inflammatory phenotype.[8] A dysregulation of this immunosurveillance function is considered to play a role in amyotrophic lateral sclerosis, Alzheimer disease, and spinal cord injury.[8,34,35] In contrast with this protective role, in the EAE model of MS, the CP immune trafficking pathway allows the initial entry of encephalitogenic T-Helper (TH)-17 lymphocytes through a CCR6-CCL20 interaction.[9] Converging evidence supports an involvement of the CCR6-CCL20 axis at the CP level in patients with MS, as they showed a much higher expression of CCR6 in cells from the CSF than do the cells from peripheral blood on memory T cells,[9] $CD161^{high}$ γδ T cells[36] and TH-1-like TH17 cells.[37]

These previous basic science findings, taken together with our results showing a correlation between CP volume and WM lesion load and ARR in RRMS, argue for a role of the CP interface in the pathogenesis of the inflammatory events of MS. Whether the CP alterations are an early triggering event, an enhancer of inflammation, or a secondary consequence of lesional activity remains however to be further explored in vivo. By contrast, CP volume did not correlate with disability scores, possibly due to the poor correlation generally found between EDSS and inflammatory disease markers in cross-sectional studies, and to the small changes in EDSS scores in the short follow-up.

The lack of a clear separation between patients with MS and controls regarding CP volumes may limit the use of this metric as a diagnostic biomarker. However, the relationship demonstrated between CP volumes and brain inflammation opens the perspective to use volumetric analysis of CPs as a biomarker of disease-related inflammatory activity, an application that should be further assessed in prospective studies.

Some limitations must be considered. First, TSPO tracer mainly targets microglia-macrophages (although not selectively[38]), and does not capture the complexity of immune cells involved in MS pathophysiology. Moreover, this correlative cross-sectional imaging study does not allow to affirm a causal relationship between CP enlargement, parenchymal immune cell activation and neurodegeneration. Longitudinal imaging studies will be needed to define whether CP volume remains stable or rather evolves over the course of the disease, and whether this metric could be used as a predictor of future inflammatory activity. Lastly, on a methodological viewpoint, a more reliable quantitative assessment of CP gadolinium uptake would benefit of dynamic contrast-enhanced scans, as previously applied for acute WM lesions.[39]

Despite these limitations, our findings of *in vivo* volumetric and inflammatory changes of the choroid plexuses in patients with multiple sclerosis (MS) are compatible with their involvement in the pathophysiology of the disease, as suggested by prior basic science works, particularly in relapsing-remitting patients with an inflammatory profile.

Acknowledgments

We warmly thank Mattia Veronese for fruitful discussion and technical help, and François-Xavier Lejeune for the statistical support. We are also thankful to Christine Baron, Christine Manciot, Bertrand Kuhnast, Vincent Lebon (SHFJ, CEA), Geraldine Gourbil (CIC) for their invaluable assistance, the staff of the CENIR (Research neuroimaging unit of the ICM), and the staff of the Unité de Recherche Clinique of Pitié Salpêtrière, in particular Anne Bissery.

The clinical studies analyzed in this article were sponsored by APHP (Assistance Publique des Hopitaux de Paris) and have benefited from the following funding: ANR (Agence Nationale de la Recherche), grant MNP2008-007125; ELA (European Leukodystrophy Association, grant 2007-0481); INSERM-DHOS (grant 2008-recherche clinique et translationnelle); Programme Hospitalier de Recherche Clinique (PHRC national, 2010; APHP); Investissements d'avenir ANR-10-IAIHU-06. They benefited additional funding from Foundation ARSEP, ECTRIMS, JNLF (Journées de Neurologie de Langue Française), FRM (Fondation pour la Recherche Médicale), and the Bouvet-Labruyére prize through the Fondation de France. This work was performed on a platform member of the France Life Imaging network (grant ANR-11-INBS-0006).

Author Contributions

V.A.G.R., M.T. and B.S. conceived and designed the study. M.B., P.G., C.L., B.B. and B.S. contributed to subject enrolment and data acquisition. V.A.G.R., E.M., A.C., M.T., M.H., E.P., B.B. and B.S. contributed to data analysis. V.A.G.R. and M.T. supervised the statistical analysis. V.A.G.R., E.M., M.T. and M.H. prepared the tables and figures. V.A.G.R., M.T., B.B. and B.S. wrote the manuscript.

Disclosures of Conflicts of Interest

The authors declared no conflict of interest related to this work.

V.A.G.R. reports fees for traveling from Novartis and Roche. E.M., A.C., M.T., M.H., E.P., M.B. and P.G. report no disclosures. C.L. has received consulting or travel fees from Biogen, Novartis, Roche, Sanofi, Teva and Merck Serono, none related to the present work. B.B. reports fees for traveling and speaker's honoraria from Novartis, Genzyme, Roche and Merck Serono, all outside of the submitted work. B.S. reports grants and personal fees for lectures from Roche, Sanofi-Genzyme, and Merck-Serono, personal fees for lectures from Novartis, Biogen and Teva, all outside of the submitted work.

References

1. Reich DS, Lucchinetti CF, Calabresi PA. Multiple sclerosis. N Engl J Med 2018;378:169–180.

2. Hemmer B, Kerschensteiner M, Korn T. Role of the innate and adaptive immune responses in the course of multiple sclerosis. Lancet Neurol 2015;14:406–419.

3. Baecher-Allan C, Kaskow BJ, Weiner HL. Multiple Sclerosis: Mechanisms and Immunotherapy. Neuron 2018;97:742–768.

4. Vidaurre OG, Haines JD, Katz Sand I, et al. Cerebrospinal fluid ceramides from patients with multiple sclerosis impair neuronal bioenergetics. Brain 2014;(Pt 8):2271-2286.

5. Wentling M, Lopez-Gomez C, Park H-J, et al. A metabolic perspective on CSF-mediated neurodegeneration in multiple sclerosis. Brain 2019;142:2756–2774.

6. Kaur C, Rathnasamy G, Ling E-A. The Choroid Plexus in Healthy and Diseased Brain. J Neuropathol Exp Neurol 2016;75:198-213.

7. Ghersi-Egea JF, Strazielle N, Catala M, et al. Molecular anatomy and functions of the choroidal blood-cerebrospinal fluid barrier in health and disease. Acta Neuropathol 2018;135:337–361.

8. Schwartz M, Baruch K. The resolution of neuroinflammation in neurodegeneration: Leukocyte recruitment via the choroid plexus. EMBO J 2014;33:7–22.

9. Reboldi A, Coisne C, Baumjohann D, et al. C-C chemokine receptor 6-regulated entry of TH-17 cells into the CNS through the choroid plexus is required for the initiation of EAE. Nat Immunol 2009;10:514–523.

10. Schmitt C, Strazielle N, Ghersi-Egea JF. Brain leukocyte infiltration initiated by peripheral inflammation or experimental autoimmune encephalomyelitis occurs through pathways connected to the CSF-filled compartments of the forebrain and midbrain. J Neuroinflammation 2012;9:187.

11. Rodríguez-Lorenzo S, Konings J, Van Der Pol S, et al. Correction to: Inflammation of the choroid plexus in progressive multiple sclerosis: Accumulation of granulocytes and T cells. Acta Neuropathol Commun 2020;8:24.

12. Vercellino M, Votta B, Condello C, et al. Involvement of the choroid plexus in multiple sclerosis autoimmune inflammation: A neuropathological study. J Neuroimmunol 2008;199:133–141.

13. Kooij G, Kopplin K, Blasig R, et al. Disturbed function of the blood-cerebrospinal fluid barrier aggravates neuro-inflammation. Acta Neuropathol 2014;128:267–277.

14. Tadayon E, Pascual-Leone A, Press D, Santarnecchi E. Choroid plexus volume is associated with levels of CSF proteins: relevance for Alzheimer's and Parkinson's disease. Neurobiol Aging 2020;89:108–117.

15. Lizano P, Lutz O, Ling G, et al. Association of Choroid Plexus Enlargement With Cognitive, Inflammatory, and Structural Phenotypes Across the Psychosis Spectrum. Am J Psychiatry 2019;176:564–572.

16. Dixon GA, Pérez CA. Multiple Sclerosis and the Choroid Plexus: Emerging Concepts of Disease Immunopathophysiology. Pediatr Neurol 2020;103:65–75.

17. Kim H, Lim Y-M, Kim G, et al. Choroid plexus changes on magnetic resonance imaging in multiple sclerosis and neuromyelitis optica spectrum disorder. J Neurol Sci 2020;415:116904.

18. Bodini B, Poirion E, Tonietto M, et al. Individual mapping of innate immune cell activation is a candidate marker of patient-specific trajectories of disability worsening in Multiple Sclerosis. J Nucl Med 2020;61:1043-1049.

19. Airas L, Rissanen E, Rinne JO. Imaging neuroinflammation in multiple sclerosis using TSPO-PET. Clin Transl Imaging 2015;3:461–473.

20. Owen DRJ, Gunn RN, Rabiner EA, et al. Mixed-Affinity Binding in Humans with 18-kDa Translocator Protein Ligands. J Nucl Med 2011;52:24–32.

21. Jenkinson M, Smith S. A global optimisation method for robust affine registration of brain images. Med Image Anal 2001;5:143–156.

22. Horsburgh A, Kirollos RW, Massoud TF. Bochdalek's flower basket: applied neuroimaging morphometry and variants of choroid plexus in the cerebellopontine angles. Neuroradiology 2012;54:1341-1346.

23. García-Lorenzo D, Lavisse S, Leroy C, et al. Validation of an automatic reference region extraction for the quantification of [18F]DPA-714 in dynamic brain PET studies. J Cereb Blood Flow Metab 2018;38:333-346.

24. Hirvonen J, Kreisl WC, Fujita M, et al. Increased in Vivo Expression of an Inflammatory Marker in Temporal Lobe Epilepsy. J Nucl Med 2012;53:234-240.

25. Mertens K, Ham H, Deblaere K, et al. Distribution Patterns of 18F-labelled Fluoromethylcholine in Normal Structures and Tumors of the Head: A PET/MRI Evaluation. Clin Nucl Med 2012;37:e196-203.

26. Thomas BA, Cuplov V, Bousse A, et al. PETPVC: A Toolbox for Performing Partial Volume Correction Techniques in Positron Emission Tomography. Phys Med Biol 2016;61:7975-7993.

27. Ling EA, Kaur C, Lu J. Origin, Nature, and Some Functional Considerations of Intraventricular Macrophages, With Special Reference to the Epiplexus Cells. Microsc Res Tech 1998;41:43-56.

28. Steffen BJ, Breier G, Butcher EC, et al. ICAM-1, VCAM-1, and MAdCAM-1 are expressed on choroid plexus epithelium but not endothelium and mediate binding of lymphocytes in vitro. Am J Pathol 1996;148:1819–1838.

29. Rodríguez-Lorenzo S, Ferreira Francisco DM, Vos R, et al. Altered secretory and neuroprotective function of the choroid plexus in progressive multiple sclerosis. Acta Neuropathol Commun 2020;8:35.

30. Betlazar C, Harrison-Brown M, Middleton RJ, et al.Cellular Sources and Regional Variations in the Expression of the Neuroinflammatory Marker Translocator Protein (TSPO) in the Normal Brain. Int J Mol Sci 2018;19:2707.

31. Cosenza-Nashat M, Zhao ML, Suh HS, et al. Expression of the translocator protein of 18 kDa by microglia, macrophages and astrocytes based on immunohis- tochemical localization in abnormal human brain. Neuropathol Appl Neurobiol 2009;35:306–328.

32. Guo Y, Weigand SD, Popescu BF, et al. Pathogenic implications of cerebrospinal fluid barrier pathology in neuromyelitis optica. Acta Neuropathol 2017;133:597–612.

33. Lauro C, Limatola C. Metabolic Reprograming of Microglia in the Regulation of the Innate Inflammatory Response. Front Immunol 2020;11:493.

34. Kunis G, Baruch K, Rosenzweig N, et al. IFN-γ-dependent activation of the brain's choroid plexus for CNS immune surveillance and repair. Brain 2013;136(Pt 11):3427-3440.

35. Kunis G, Baruch K, Miller O, Schwartz M. Immunization with a Myelin-Derived Antigen Activates the Brain's Choroid Plexus for Recruitment of Immunoregulatory Cells to the CNS and Attenuates Disease Progression in a Mouse Model of ALS. J Neurosci 2015;35:6381-6393.

36. Schirmer L, Rothhammer V, Hemmer B, Korn T. Enriched CD161high CCR6+ γδ T cells in the cerebrospinal fluid of patients with multiple sclerosis. JAMA Neurol 2013;70:345-351.

37. van Langelaar J, van der Vuurst de Vries RM, Janssen M, et al. T helper 17.1 cells associate with multiple sclerosis disease activity: perspectives for early intervention. Brain 2018;141:1334-1349.

38. Nutma E, Stephenson JA, Gorter RP, et al. A quantitative neuropathological assessment of translocator protein expression in multiple sclerosis. Brain 2019;142:3440–3455.
39. Absinta M, Sati P, Gaitán MI, et al. Seven-tesla phase imaging of acute multiple sclerosis lesions: a new window into the inflammatory process. Ann Neurol 2013;74:669-678.

Demographic and imaging characteristics					
Characteristic	**HC**	**Whole MS group**	**RRMS**	**PMS**	***P***
Number (female)	44 (23)	97 (49)	61 (31)	36 (18)	.47
Age (yrs), mean [SD]	39 [14]	42 [12]	37 [10]	50 [11]	.18
Disease duration (yrs), median (range)	–	4.8 (0.1-23)	4 (0.1-23)	6.5 (0.3-22)	.04
EDSS, median (range)	–	3 (0-7.5)	2 (0-6)	6 (2.5-7-5)	<.001
EDSS change, median (range)	–	0 (-3:2)	0 (-3:2)	1 (0:2)	
Treatment at study entry, no. of patients	–	No treatment = 40 First-line treatment = 37 Second-line treatment = 20	No treatment = 10 First-line treatment = 36 Second-line treatment = 15	No treatment = 30 First-line treatment = 1 Second-line treatment = 5	<.001
Clinically active disease (defined as 2-year retrospective ARR≠0), no. of patients	–	55	49	6	
2-year retrospective ARR, mean [SD]	–	0.6 [0.72]	0.86 [0.74]	0.15 [0.41]	
2-year prospective ARR, mean [SD]	–	0.19 [0.45]	0.22 [0.39]	0.15 [0.5]	
4-year cumulative ARR, mean [SD]	–	0.39 [0.48]	0.53 [0.47]	0.15 [0.42]	
Total intracranial volume (ml), mean [SD]	1482 [165]	1488 [149]	1471 [148]	1514 [150]	
T2-w lesion load (ml), mean [SD]	–	15.72 [15.13]	16.44 [16.90]	15.08 [11.79]	
T2-w lesion load (ratio of TIV), mean [SD]	–	10.6×10^{-3} [10.5×10^{-3}]	11.2×10^{-3} [11.7×10^{-3}]	10×10^{-3} [8.2×10^{-3}]	
Number of gadolinium-enhancing lesions, mean [SD] (no. of patients)	–	2.1 [6.2] (31)	3.3 [7.5] (26)	0.6 [0.5] (5)	
Whole brain volume (ml), mean [SD]	957 [118]	924 [104]	924 [104]	923 [106]	
Whole brain volume (ratio of TIV), mean [SD]	0.65 [0.02]	0.62 [0.03]	0.63 [0.04]	0.61 [0.03]	
Thalamic volume (ml), mean [SD]	14.67 [1.99]	12.80 [1.76]	12.80 [1.83]	12.76 [1.67]	

Thalamic volume (ratio of TIV), mean [SD]	9.9×10^{-3} [0.7×10^{-3}]	8.6×10^{-3} [1×10^{-3}]	8.7×10^{-3} [1×10^{-3}]	8.4×10^{-3} [1×10^{-3}]	
WM (NAWM) volume (ml), mean [SD]	250.36 [175.85]	64.06 [32.10]	62.14 [32.15]	66.29 [32.20]	
WM (NAWM) volume (ratio of TIV), mean [SD]	0.17 [0.12]	0.04 [0.02]	0.04 [0.02]	0.04 [0.02]	
Cortex volume (ml), mean [SD]	471 [51]	455 [48]	460 [49]	447 [47]	
Cortex volume (ratio of TIV), mean [SD]	0.32 [0.02]	0.31 [0.02]	0.31 [0.02]	0.30 [0.01]	

Table 1: Demographic and MRI characteristics of the analyzed study sample.

Volumes are expressed in ml and as ratio of total intracranial volume (TIV). HC = healthy controls; MS = multiple sclerosis; RRMS = relapsing-remitting multiple sclerosis; PMS= progressive multiple sclerosis; ARR= annualized relapse rate; SD = standard deviation; EDSS = Extended Disability Status Scale; T2-w = T2-weghted; TIV= total intracranial volume; WM= white matter of healthy controls; NAWM= normal-appearing white matter, defined as the WM without lesions and perilesions.

	GROUP	STATISTICS	VOLUMES (ratio of TIV)			
			WHOLE BRAIN VOLUME	THALAMIC VOLUME	WM (NAWM) VOLUME	CORTEX VOLUME
CHOROID PLEXUS VOLUME (ratio of TIV)	HC	*coeff*	-16.84	-0.11	6.27	4.43
		95% CI	-36.47 2.79	-0.82 0.60	-105.77 118.31	-9.73 18.59
		P	**.18**	**>.99**	**>.99**	**>.99**
	WHOLE MS GROUP	*coeff*	-26.87	-0.57	-12.49	1.45
		95% CI	-44.85 -8.90	-1.04 -0.10	-21.02 -3.96	-6.74 9.64
		P	**.004**	**<.001**	**.004**	**>.99**
	RRMS	*coeff*	-23.69	-0.76	-12.73	-1.59
		95% CI	-42.73 -4.65	-1.24 -0.28	-21.50 -3.97	-9.92 6.75
		P	.02	.002	.005	.71
	PMS	*coeff*	-30.70	-0.24	-12.12	7.94
		95% CI	-56.96 -4.45	-0.89 0.42	-23.93 -0.31	-3.51 19.39
		P	.02	.48	.004	.17

Table 2: Association between CP volume and volumes of specific brain regions, in all patients with MS, in RRMS and PMS subgroups, and in HCs. All volumes were expressed as ratio of total intracranial volume (TIV). In the multivariable regression model, CP volume was set as independent variable and each one of the other volumes was in turn set as dependent variable, adjusting for age, sex, MRI scanner, whole brain volume (except when this was set as dependent variable) and treatment (only in patients). *p*-values were Bonferroni corrected for the correlations within whole MS and the HC groups (bold), but not for the correlations within RRMS and PMS subgroups. MS = multiple sclerosis; TIV = total intracranial volume; RRMS = relapsing-remitting MS; PMS = progressive MS; HC =

healthy controls; WM = white matter of HC; NAWM = normal-appearing white matter of MS; *coeff*: multivariable regression coefficient; CI= confidence interval; T2-w = T2-weighted; *P* = p-value.

	GROUP	STATISTICS	THALAMIC DVR	WM (NAWM) DVR	CORTEX DVR	T2-w LESION DVR	PERILESION DVR
CHOROID PLEXUS VOLUME (ratio of TIV)	**HC**	*coeff*	190.98	112.42	96.91	-	-
		95% CI	-22.76 404.81	-4.25 229.10	-60.08 254.03	-	-
		P	**.10**	**.07**	**.38**	-	-
	WHOLE MS GROUP	*coeff*	269.62	87.12	50.30	44.19	53.07
		95% CI	7.48 531.65	19.19 155.05	-72.28 172.88	-116.93 205.30	-93.55 199.70
		P	**.04**	**.005**	**>.99**	**>.99**	**>.99**
	RRMS	*coeff*	89.51	76.12	5.60	136.14	73.77
		95% CI	-124.73 303.74	22.69 129.55	-174.10 185.30	8.52 263.77	-48.79 196.34
		P	.40	.007	.95	.04	.23
	PMS	*coeff*	341.42	92.51	67.99	8.20	46.67
		95% CI	146.22 536.61	32.85 152.18	-34.69 170.67	-151.59 167.99	-82.72 176.06
		P	.001	.004	.19	.92	.47

Table 3: Association between CP volume and ^{18}F-DPA-714 DVR of specific brain regions, in all patients with MS, in RRMS and PMS subgroups, and in HCs. CP volume was expressed as ratio of total intracranial volume (TIV). In the multivariable regression model, CP volume was set as independent variable and each DVR value in the selected volumes was in turn set as dependent variable, adjusting for age, sex, TSPO affinity, treatment (only in patients) and whole brain volume. *p*-values were Bonferroni corrected for the correlations within whole MS and the HC groups, (bold), but not for the correlations within RRMS and PMS subgroups. TIV = total intracranial volume; MS = multiple sclerosis; RRMS = relapsing-remitting MS; PMS = progressive MS; HC = healthy controls; DVR = distribution volume ratio; WM = white matter of HC; NAWM = normal-appearing white matter of MS; *coeff*: multivariable regression coefficient; CI= confidence interval; T2-w = T2-weighted; *P* = p-value;

Figures

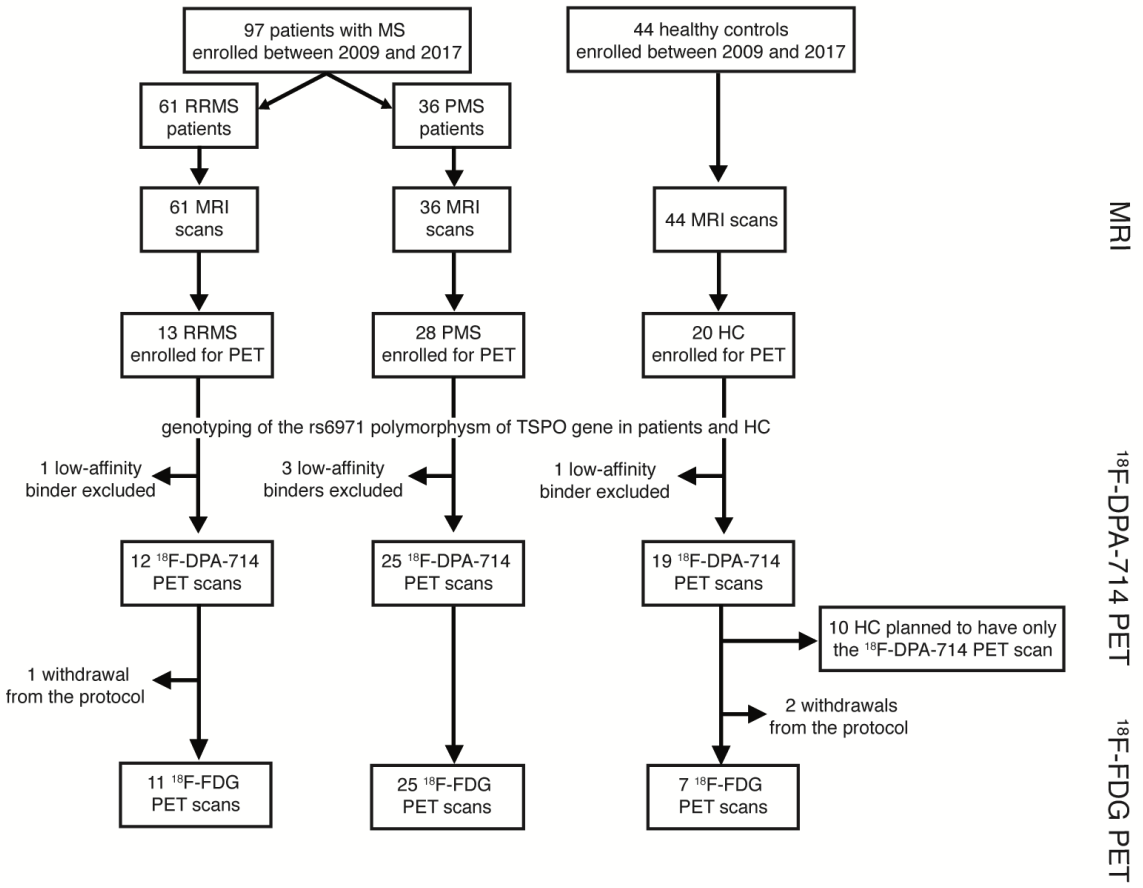

Figure 1: Flow diagram showing the initial number of participants and those excluded/lost for any reasons.

MS = multiple sclerosis; RRMS = relapsing-remitting multiple sclerosis; PMS = progressive multiple sclerosis; HC = healthy controls; TSPO = translocator protein; FDG = fluorodeoxyglucose.

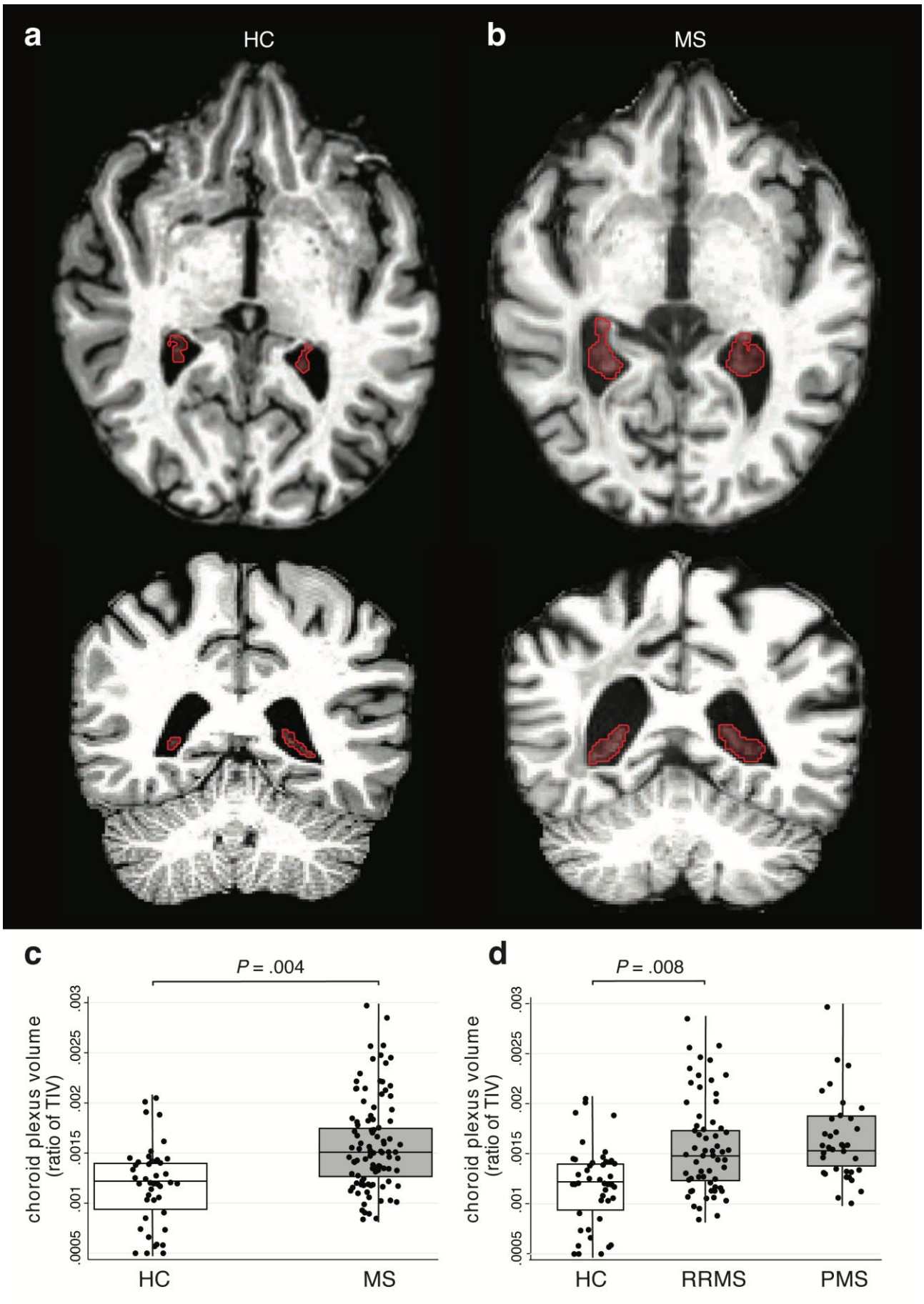

Figure 2: Choroid plexus volume is greater in MS compared with HCs.

(a-b) Non-enhanced 3D T1-weighted MPRAGE images (TR/TE: 2300/2.98 ms) showing the segmentation of the left and right choroid plexus (red) on the axial (top) and coronal (bottom) plane in a HC (**a**) and a patient with MS (**b**). **(c-d)** Box plots showing higher choroid plexus volume in patients with MS *versus* HCs (**c**), and in RRMS or patients with PMS separately *versus* HC (**d**). CP volume was normalized on total intracranial volume. HC = healthy controls; MS = multiple sclerosis; RRMS = relapsing-remitting multiple sclerosis; PMS = progressive multiple sclerosis; TIV = total intracranial volume; *P* = p value.

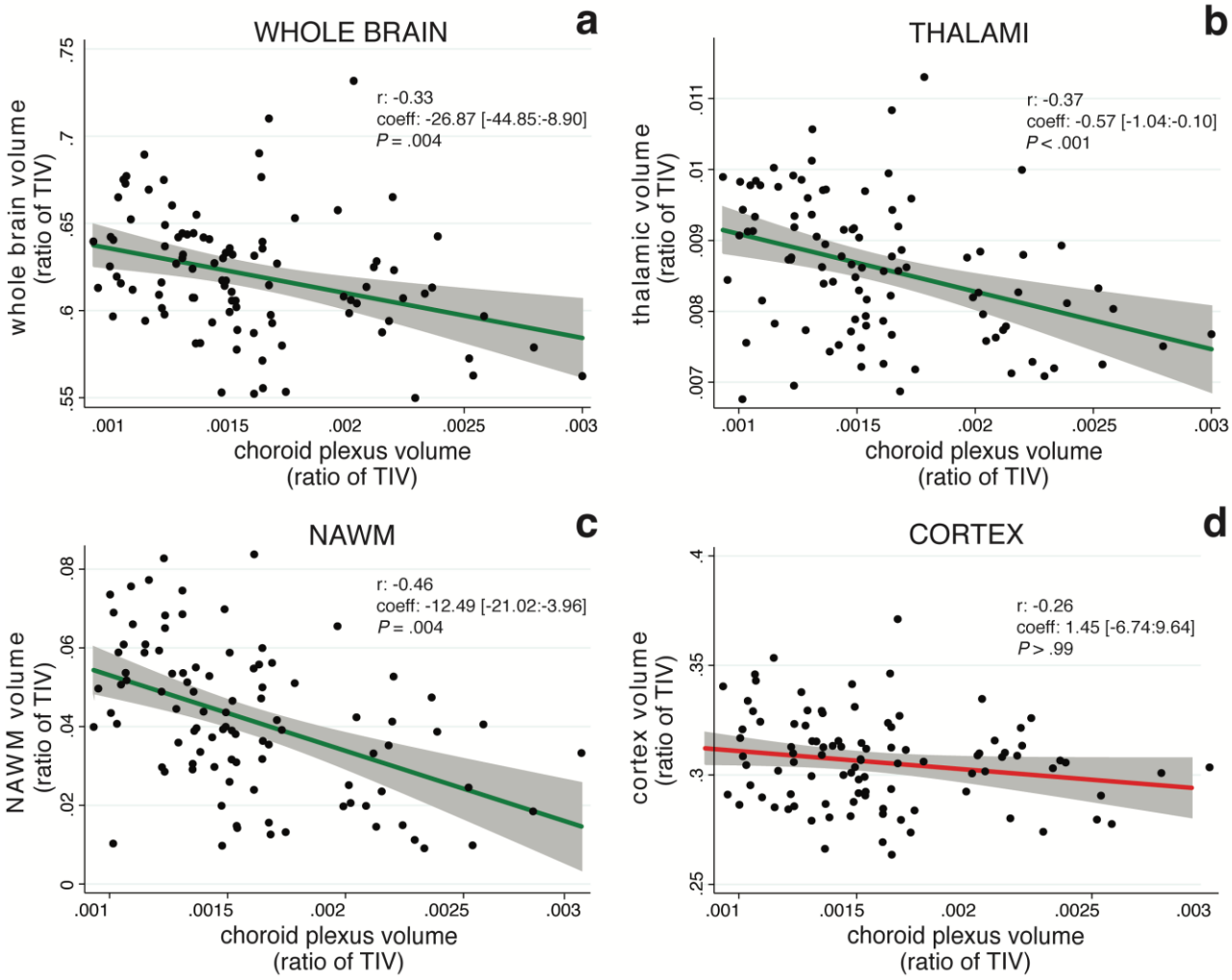

Figure 3: Correlation between choroid plexus volume and brain tissue volumes in MS.

(a-d) Scatter plots showing the significant negative association between choroid plexus volume and whole brain volume (**a**), thalamic volume (**b**), NAWM volume (**c**), and the nonsignificant association between choroid plexus volume and cortical volume (**d**). The fit line is colored in green for significant associations and in red for non-significant associations. All volumes were normalized on total intracranial volume. In the multivariable regression model, CP volume was set as independent variable and each one of the other

volumes was in turn set as dependent variable, adjusting for age, sex, MRI scanner, treatment and whole brain volume (except when this was set as dependent variable). Confidence intervals are indicated in square brackets and represented by the grey areas on the graphs. NAWM = normal-appearing white matter; TIV = total intracranial volume r = Pearson's r; coeff = multivariable regression coefficient; *P* = p value.

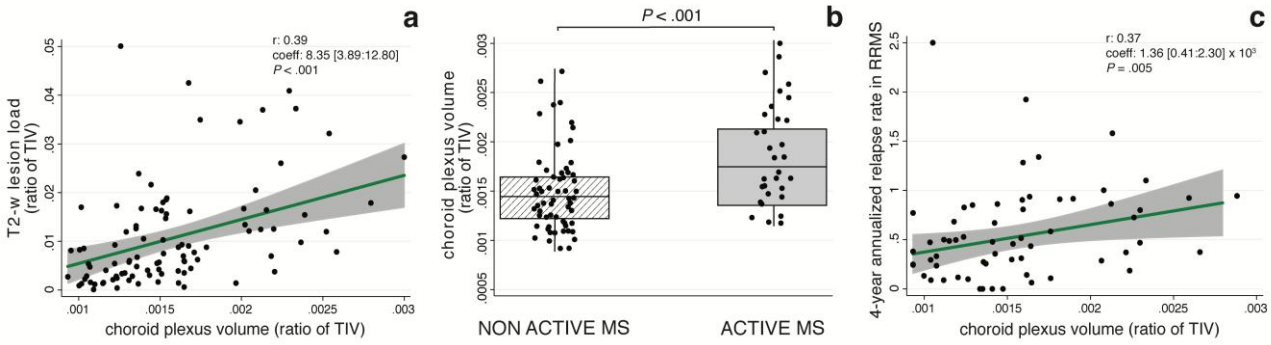

Figure 4: Larger choroid plexuses in active MS, correlation with T2 lesion load and annualized relapse rate.

(a) Scatter plot of the association between higher choroid plexus volume and greater T2 lesion load in MS patients. **(b)** Box plot showing that MS patients with at least one gadolinium-enhancing lesion had larger choroid plexuses compared with MS patients without active MRI lesions. **(c)** Scatter plot showing the significant positive association between 4-year annualized relapse rate, reflecting the extent of clinical disease activity, and choroid plexus volume in RRMS. All volumes were normalized on total intracranial volume. Confidence intervals are indicated in square brackets and represented by the grey areas on the graphs. MS = multiple sclerosis; RRMS = relapsing-remitting multiple sclerosis; T2-w = T2-weighted; TIV = total intracranial volume; r = Pearson's r; coeff = multivariable regression coefficient; *P* = p value.

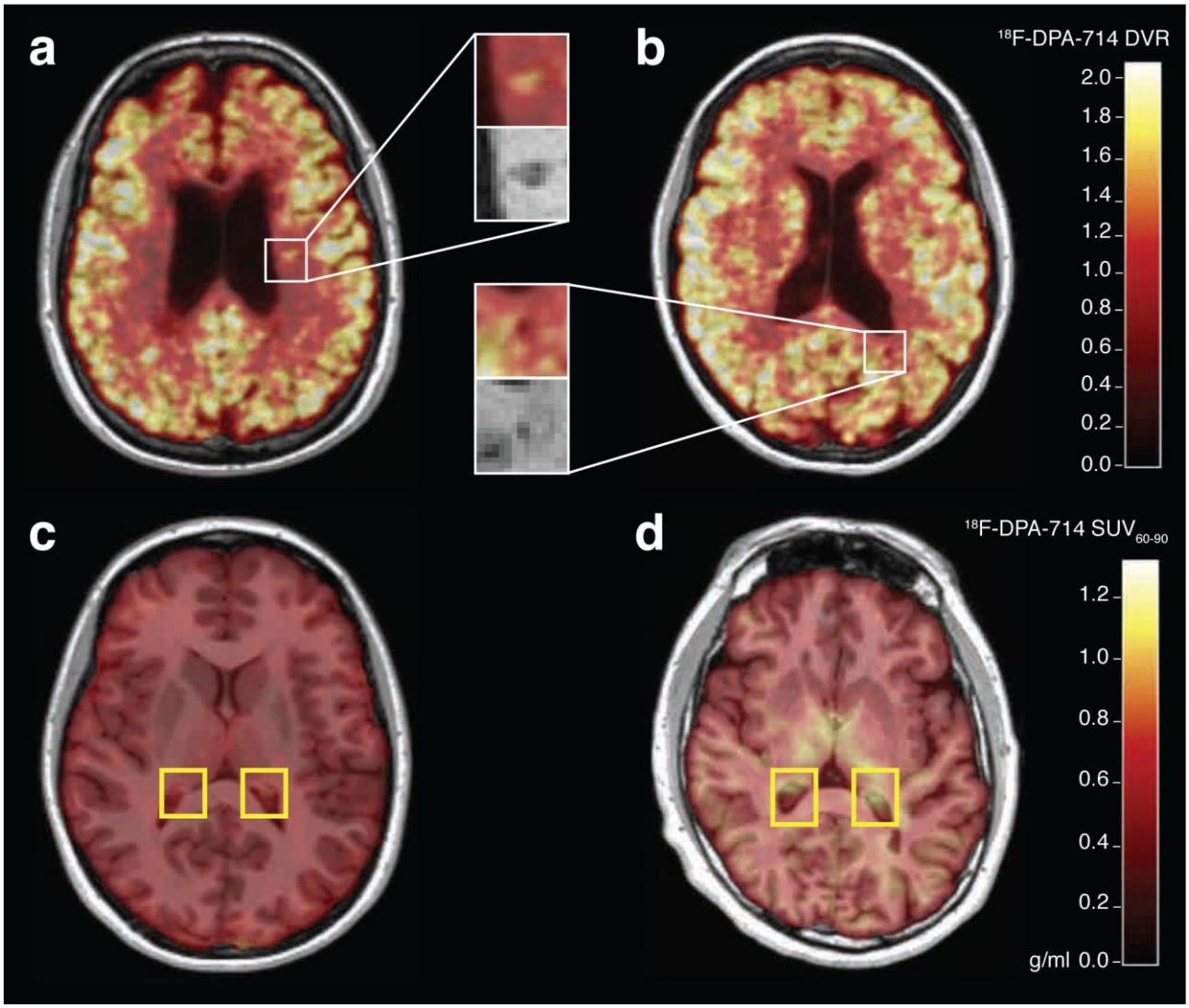

Figure 5: ^{18}F-DPA-714 DVR and ^{18}F-DPA-714 SUV$_{60\text{-}90}$ maps in patients with MS and HC.

(a-b) ^{18}F-DPA-714 distribution volume ratio (DVR) maps (axial plane) from a HAB patient with MS, showing high DVR signal inside an MS lesion (magnification in both PET [top] and non-enhanced 3D-T1 MPRAGE MRI [bottom, TR/TE: 2300/2.98 ms], **a**) and a perilesional area (magnification in both PET [top] and non-enhanced 3D-T1 MPRAGE MRI [bottom, TR/TE: 2300/2.98 ms], **b**). **(c-d)** ^{18}F-DPA-714 standardized uptake value (SUV$_{60\text{-}90}$) maps (axial plane) of a HAB HC (**c**) and a HAB patient with MS (**d**). Both of which have a SUV in the choroid plexuses which corresponds to the median value within their group. Choroid plexuses (yellow box) of MS show higher ^{18}F-DPA-714 SUV$_{60\text{-}90}$ compared with HC. HC = healthy controls; MS = multiple sclerosis. DVR = distribution volume ratio; SUV$_{60\text{-}90}$ = standardized uptake value between 60 and 90 minutes of acquisition.

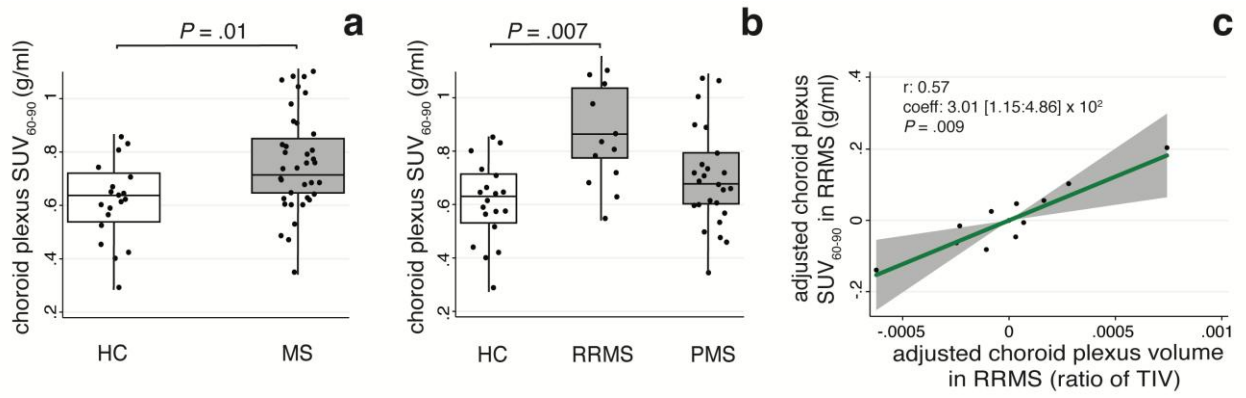

Figure 6: Choroid plexus inflammation is higher in MS compared with HC.

(a-b) Box plot showing greater choroid plexus inflammation, measured as ^{18}F-DPA-714 $SUV_{60\text{-}90}$, in patients with MS *versus* HCs (**a**), and in RRMS or patients with PMS separately *versus* HC (**b**). **(c)** Added variable plot showing the association between volume and inflammation in the choroid plexuses of patients with RRMS. CP volume was normalized on total intracranial volume. Confidence intervals are indicated in square brackets and represented by the grey areas on the graphs. $SUV_{60\text{-}90}$ = standardized uptake value between 60 and 90 minutes of acquisition; HC = healthy controls; MS = multiple sclerosis; RRMS = relapsing-remitting multiple sclerosis; PMS = progressive multiple sclerosis; TIV = total intracranial volume; r = Pearson's r; coeff = multivariable regression coefficient; *P*= p value.

Supplemental 1

MRI protocol

Acquisition parameters were identical for Siemens TRIO and PRISMA 3T systems, and acquired sequences included:

1) 3D T1-weighted magnetization-prepared rapid gradient echo (3D-T1 MPRAGE: repetition time (TR)/echo time (TE): 2300/2.98 ms, inversion time: 900 ms, resolution: 1.0x1.0x1.1mm^3);

2) T2-weighted (T2-w): TR/TE: 4100/83 ms, resolution: 0.9x0.9x3.0mm^3);

3) pre- and post-gadolinium T1 spin-echo (TR/TE: 700/14 ms, resolution: 1.0x1.0x3.0mm^3).

PET acquisition and quantification

^{18}F-DPA-714 PET and 18F-FDG PET exams were performed on a 3D high-resolution research tomograph (HRRT; CPS Innovations, Knoxville, TN). The HRRT is a dedicated brain imaging system with a 31.2 cm transaxial and 25.5 cm axial field of view.

^{18}F-DPA-714 PET acquisition: After a transmission scan using a ^{137}Cs point source, the 90-minute emission scan was initiated with a 1-minute intravenous bolus injection of ^{18}F-DPA-714 (mean 198.4±22.9MBq). Images were reconstructed using the 3D ordinary Poisson ordered subset expectation maximization algorithm. An additional smoothing filter implementing the point spread function, which has been shown to be effective in reducing the effect of partial volume in PET data, was applied on the reconstructed images, achieving an intra-slice spatial resolution of ~2.5mm full width at half maximum. All the resulting dynamic PET images consisted of 27 time interval images (time frames): six 1min frames for the initial 6 minutes (6x1), followed by 7x2-, and 14x5-minute frames, with a voxel size of 1.22x1.22x1.22mm^3.

^{18}F-FDG PET acquisition: The 60-min emission scan was initiated with a 1-minute intravenous bolus injection of 18F-FDG (mean = 191±8.5 MBq). All the resulting dynamic PET images consisted of 7 time

frames: one 30-minute initial frame (1x30), followed by 6x5-minute frames, with a voxel size of 1.22x1.22x1.22mm^3.

Reconstructed dynamic PET data of all subjects were realigned for motion correction according to the process of frame-to-reference image registration using SPM, v8. In particular, the first PET frame was excluded as it did not contain enough spatial information to be correctly aligned. Motion correction was then performed with a two-step procedure: all frames were first aligned to the second frame through a rigid transformation, and then all frames were registered to the mean of the frames obtained after the first realignment.

Voxel-wise ^{18}F-DPA-714 distribution volume ratio (DVR) parametric maps were calculated using the simplified version of the Logan graphical method based on reference region, which omits the term (k2') representing the tissue-to-plasma clearance of the reference tissue. The reference region was extracted using a supervised clustering algorithm as detailed in ref 23, while the linear start time of the Logan plot was taken at 20min.

^{18}F-DPA-714 and ^{18}F-FDG uptake in the choroid plexuses

^{18}F-DPA-714 and ^{18}F-FDG uptake in the choroid plexuses was defined as the average standardized uptake value (SUV) inside the CPs. The use of SUV instead of DVR relies on the fact that the assumptions for Logan graphical analysis with reference region were not respected in this case (given the different kinetics of tracer exchange between the blood and the tissue in the CPs, and the absence of a blood-brain barrier).
SUV maps of ^{18}F-DPA-714 were calculated from the frames of the last 30 minutes of acquisition (SUV_{60-90}) as the radioactivity concentration divided by injected dose per body mass.
SUV maps of ^{18}F-FDG were calculated from the frames of the last 15 minutes of acquisition (SUV_{45-60}) as the radioactivity concentration divided by injected dose per body mass, multiplied by plasma glucose concentration.
Mean ^{18}F-DPA-714 SUV_{60-90} and ^{18}F-FDG SUV_{45-60} in the CPs were extracted for each subject by overlapping the CP masks to the SUV maps, after performing partial volume correction of the CPs with the single target correction method, as implemented in PETPVC.

Supplemental Figure 1

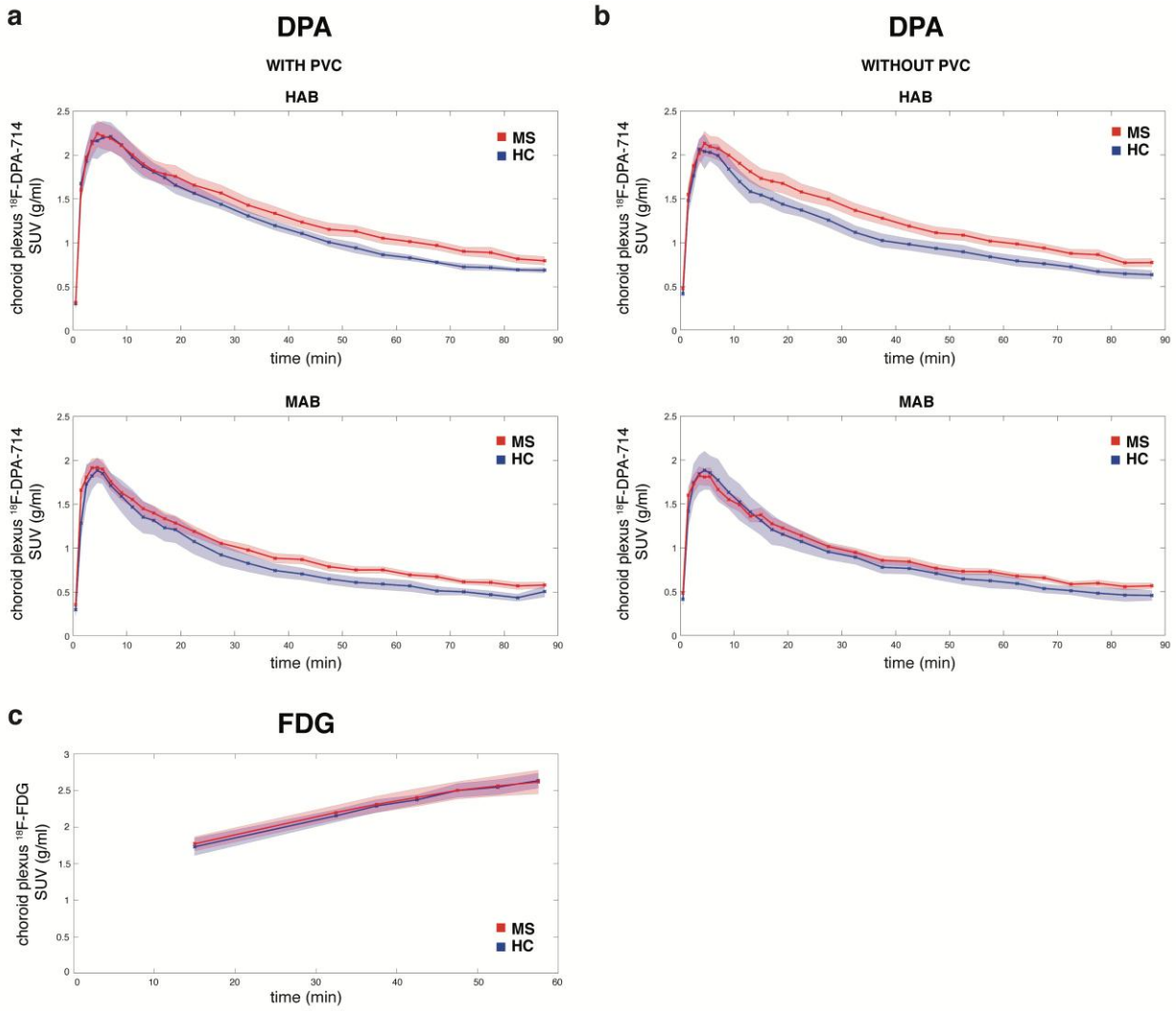

Mean ^{18}F-DPA-714 and ^{18}F-FDG SUV curves in patients with MS and HC.

(**a-b**) Mean ^{18}F-DPA-714 SUV curves over time for the whole PET scan in high- (top) and mixed-affinity binders (bottom) with (**a**) and without (**b**) partial volume correction. (**c**) Mean ^{18}F-FDG SUV curves over time for the whole PET scan in patients with MS and healthy controls, with PVC. Lines represent the mean

SUV value, while areas correspond to the standard error of the mean. PVC = partial volume correction; SUV = standardized uptake value; HAB = high-affinity binders; MAB = mixed-affinity binders; FDG = fluorodeoxyglucose; MS = multiple sclerosis; HC = healthy controls.